© 2014. Published by The Company of Biologists Ltd | Journal of Cell Science (2014) 127, 1138–1149 doi:10.1242/jcs.145052

RESEARCH ARTICLE

Phospholipid flippase ATP8A2 is required for normal visual and auditory function and photoreceptor and spiral ganglion cell survival

Jonathan A. Coleman[1,*], Xianjun Zhu[2,3,*], Hidayat R. Djajadi[1], Laurie L. Molday[1], Richard S. Smith[3], Richard T. Libby[3,4], Simon W. M. John[3,‡] and Robert S. Molday[1,5,‡]

ABSTRACT

ATP8A2 is a P_4-ATPase that is highly expressed in the retina, brain, spinal cord and testes. In the retina, ATP8A2 is localized in photoreceptors where it uses ATP to transport phosphatidylserine (PS) and phosphatidylethanolamine (PE) from the exoplasmic to the cytoplasmic leaflet of membranes. Although mutations in *ATP8A2* have been reported to cause mental retardation in humans and degeneration of spinal motor neurons in mice, the role of ATP8A2 in sensory systems has not been investigated. We have analyzed the retina and cochlea of ATP8A2-deficient mice to determine the role of ATP8A2 in visual and auditory systems. ATP8A2-deficient mice have shortened photoreceptor outer segments, a reduction in photoresponses and decreased photoreceptor viability. The ultrastructure and phagocytosis of the photoreceptor outer segment appeared normal, but the PS and PE compositions were altered and the rhodopsin content was decreased. The auditory brainstem response threshold was significantly higher and degeneration of spiral ganglion cells was apparent. Our studies indicate that ATP8A2 plays a crucial role in photoreceptor and spiral ganglion cell function and survival by maintaining phospholipid composition and contributing to vesicle trafficking.

KEY WORDS: ATP8A2, Phospholipid flippase, P4-ATPase, Photoreceptors, Visual system, Spiral ganglion cells, Auditory system

INTRODUCTION

P_4-ATPases are a family of P-type ATPases that use the energy from ATP hydrolysis to translocate or 'flip' aminophospholipids from the exoplasmic to the cytoplasmic leaflet of membranes. Flipping of aminophospholipids has been implicated in establishing phospholipid asymmetry in biological membranes and generating the membrane curvature required for many cellular processes (Coleman et al., 2013; Graham and Kozlov, 2010; Puts and Holthuis, 2009; Sebastian et al., 2012; van der Mark et al., 2013).

ATP8A2 is a member of the P_4-ATPase family of phospholipid transporters which is highly expressed in the retina, brain, spinal cord and testis (Cacciagli et al., 2010; Coleman et al., 2009; Zhu et al., 2012). It associates with CDC50A, the β-subunit crucial for the expression and flippase activity of ATP8A2 (Coleman and Molday, 2011; van der Velden et al., 2010). In the retina, a significant portion of the ATP8A2–CDC50A complex localizes to the light-sensitive photoreceptor outer segments. Biochemical studies indicate that the ATP8A2–CDC50A complex transports phosphatidylserine (PS) and to a lesser extent phosphatidylethanolamine (PE) across photoreceptor disc membranes (Coleman et al., 2009).

Mutations in *ATP8A2* are known to cause a severe neurological disorder characterized by cerebellar axatia, mental retardation and dysequilibrium syndrome (Cacciagli et al., 2010; Emre et al., 2012). Recently, the wabbler-lethal (*wl*) mouse was found to harbor a deletion in exon 22 of *Atp8a2*, which results in an inactive protein and distal axonal degeneration in spinal motor neurons (Zhu et al., 2012). Knockdown of ATP8A2 in PC12 cells indicates that the lipid transport activity of ATP8A2 influences neurite length (Xu et al., 2012). Mice deficient in ATP8A1, a homolog of ATP8A2, show an increase in externalization of PS on the plasma membranes of hippocampal cells and a deficiency in hippocampus-dependent learning (Levano et al., 2012). The function of ATP8A1 appears to partially overlap with the function of ATP8A2 because loss of activity of both transporters results in neonatal lethality (Zhu et al., 2012).

Exposure of PS on the surface of cells serves as a signal for phagocytosis (Wu et al., 2006) and is thought to play a role in outer segment turnover (Ruggiero et al., 2012). In yeast, P_4-ATPases function in vesicle budding and trafficking (Sebastian et al., 2012). Little is known about the role of mammalian P_4-ATPases in vesicle transport. However, the pathophysiology of P_4-ATPase-associated disorders suggests that this might be an evolutionarily conserved function.

The role of P_4-ATPases in sensory systems has not been previously investigated. In this study we have examined the retina and cochlea of *Atp8a2*-knockout and *wl/wl* mice to begin to define the role of ATP8A2 in the visual and auditory systems. Here, we show that ATP8A2 deficiency causes an alteration in phospholipid composition, a shortening of outer and inner segments, a reduction in the photoresponse and loss of photoreceptor cells in the visual system, and a reduction in hearing and spiral ganglion cell survival in the auditory system. Our studies suggest that ATP8A2 phospholipid flippase activity

[1]Department of Biochemistry and Molecular Biology, University of British Columbia, Vancouver, BC V6T 1Z3, Canada. [2]The Sichuan Provincial Key Laboratory for Human Disease Gene Study, Sichuan Academy of Medical Sciences & Sichuan Provincial People's Hospital, Chengdu, Sichuan 610072, China. [3]Howard Hughes Medical Institute, The Jackson Laboratory, Bar Harbor, ME 04609, USA. [4]Flaum Eye Institute, University of Rochester Medical Center, Rochester, NY 14642, USA. [5]Department of Ophthalmology and Visual Sciences, Centre for Macular Research, University of British Columbia, Vancouver, BC, V5Z 3N9, Canada.

*These authors contributed equally to this work.

‡Authors for correspondence (molday@mail.ubc.ca; Simon.John@jax.org)

Received 21 October 2013; Accepted 6 December 2013

Journal of Cell Science

Journal of Cell Science (2014) 127, 1138–1149 doi:10.1242/jcs.145052

plays a crucial role in vesicle trafficking, and neuronal function and survival in these sensory systems.

RESULTS

ATP8A2-deficient mice

An *Atp8a2*-knockout mouse was generated by replacing exons 11–13 with a *neo* cassette (Fig. 1A). Deletion of exons 11–13, which encode transmembrane segment M4 and part of the P-domain of P-type ATPases crucial for ATP8A2 structure and function, is predicted to generate an unstable product. PCR genotyping was used to identify homozygous knockout mice from their wild-type (WT) and heterozygous littermates (Fig. 1B) and RT-PCR was used to demonstrate the absence of *Atp8a2* gene expression in the retinas of homozygous knockout mice and reduced expression in heterozygous knockout mice (Fig. 1C). Western blots confirmed the absence of ATP8A2 and reduced levels of its β-subunit CDC50A in retina extracts from knockout mice (Fig. 1D). Compared with WT and heterozygous animals, *Atp8a2*-knockout mice were noticeably smaller (Fig. 1E), and exhibited labored movements and clasping of hind legs when held by the tail (Fig. 1F). The overall phenotype is highly similar to that of the *wl/wl* mouse (Zhu et al., 2012), suggesting that distal axonal degeneration of the spinal cord also occurs in the *Atp8a2*-knockout mouse. The mean survival time of 1–2 months for the *Atp8a2*-knockout mouse is also similar to that of the *wl/wl* mouse.

Localization of ATP8A2 and CDC50A in the retina of *Atp8a2*-knockout and *wl/wl* mice

The distribution of ATP8A2 and CDC50A in WT mice was compared with that in age-matched *Atp8a2* knockout and *wl/wl* mice by immunofluorescence microscopy (Fig. 2A,B). Strongest immunolabeling of ATP8A2 was observed in the outer segment layer of P23 WT mice with weaker labeling in other retinal layers including the inner segment as previously reported (Coleman

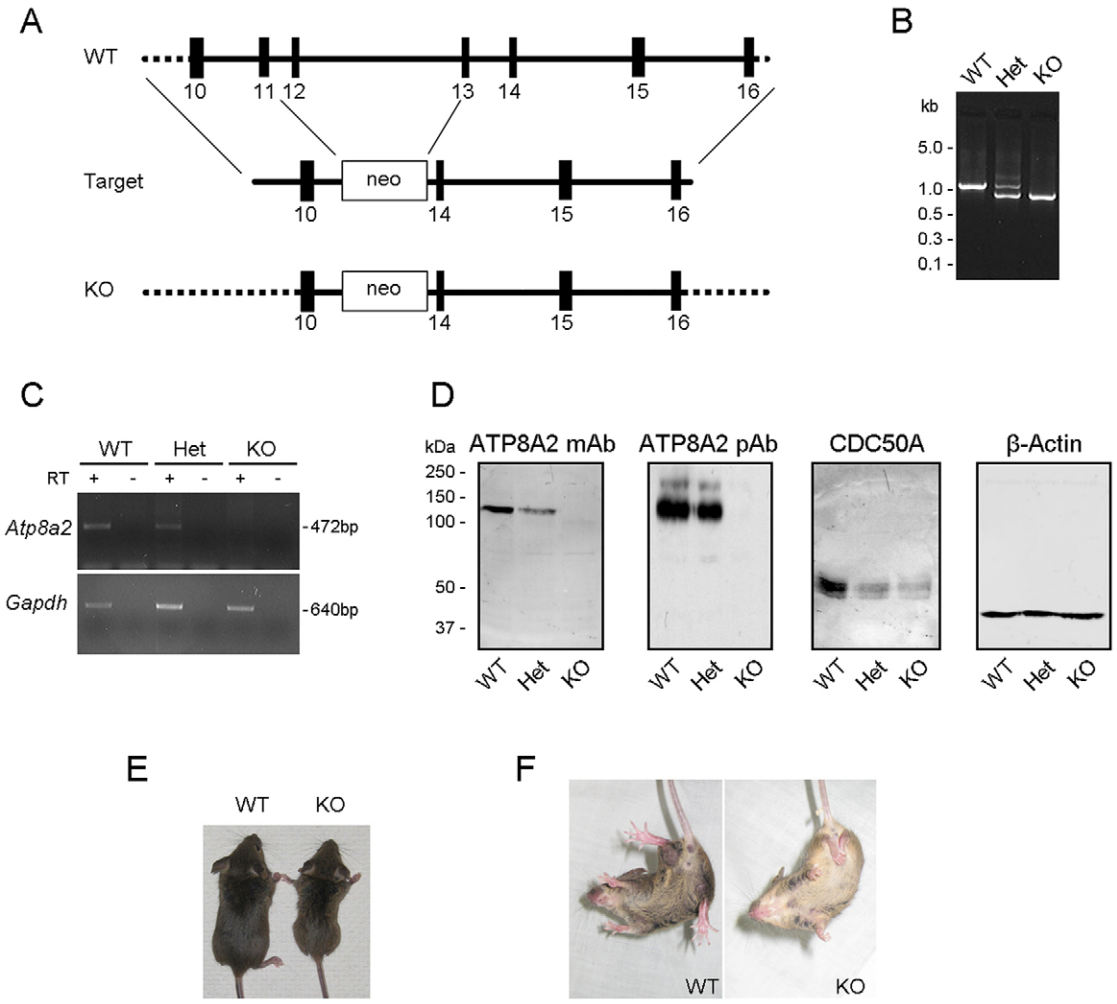

Fig. 1. Generation of the *Atp8a2*-knockout mouse. (A) Scheme showing the targeting strategy for disruption of the *Atp8a2* gene. (B) Genotyping of *Atp8a2*-knockout (KO) mice. PCR of ear punches produced distinct products of 1190 bp for the wild-type (WT) and 931 bp for the knockout mice. Both PCR products were present in the heterozygous (Het) mice. (C) RT-PCR analysis of WT and knockout mice. RT-PCR was performed using primers specific to *Atp8a2* and *Gapdh*, as a loading control. The DNA fragments were detected as a 472 bp product for *Atp8a2* and 640 bp product for *Gapdh* (+ lanes). As a negative control, the reverse transcriptase was not added (− lanes). (D) Western blots of ATP8A2 and CDC50A in wild-type (WT), and heterozygous (Het) and homozygous (KO) mice by western blotting. ATP8A2 was detected as a 130 kDa protein using the monoclonal Atp6C11 antibody (mAb) or a polyclonal antibody (pAb) and CDC50A was detected as a 50 kDa protein using the Cdc50-7F4 mAb. β-actin was used as a loading control. (E,F) Comparison of WT and knockout mice. Knockout mice (right) are easily distinguished from WT mice (left) and heterozygous littermates at three weeks because of their runted appearance (E) and clasping of hind limbs (F) when held by the tail.

Journal of Cell Science (2014) 127, 1138–1149 doi:10.1242/jcs.145052

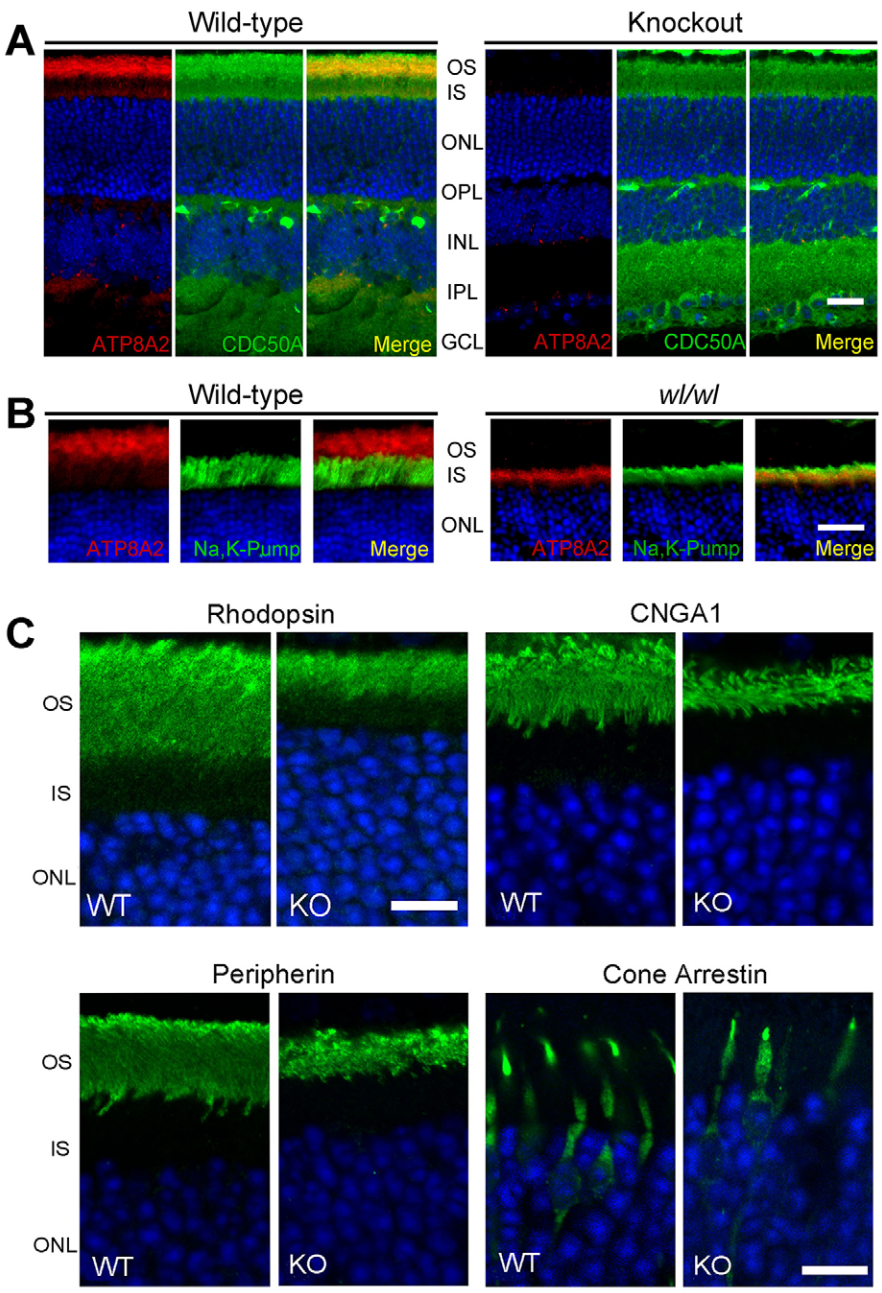

Fig. 2. Analysis of ATP8A2 and CDC50A expression in the retina of *Atp8a2*-knockout and *wl/wl* mice by immunofluorescence microscopy. (A) Immunofluorescence labeling of cryosections of retinas from a wild-type and knockout mouse at 23 days of age using the pAb to ATP8A2 (red) and a mAb against CDC50A (green). Nuclei were labeled with 4′,6-diamidino-2-phenylindole (blue). The merged image shows colocalization of ATP8A2 and CDC50A (yellow) in the OS of the wild-type mice. (B) Labeling of retina cryosections from wild-type and *wl/wl* mice at 30 days of age using a pAb against ATP8A2 (red). The inner segment (IS) is labeled with an antibody against the Na^+/K^+ pump (green). The merged image shows colocalization of ATP8A2 and the Na^+/K^+ pump in the IS of the *wl/wl* retina. (C) Immunofluorescence localization of rhodopsin, cyclic nucleotide-gated channel α-subunit (CNGA1), peripherin and cone arrestin (green) in cryosections of 23-day-old wild-type (WT) and knockout (KO) mice (green). Sections were counterstained with the nuclei stain 4′,6-diamidino-2-phenylindole (blue). These outer segment proteins appear to localize correctly in rod and cone photoreceptors of the knockout retina despite the shorter length of the outer segment. OS, outer segments; IS, inner segments; ONL, outer nuclear layer. Scale bars: 20 μm.

et al., 2009). Strong CDC50A immunoreactivity was also observed in the outer segments of WT mice with moderate labeling in other retinal layers. In contrast, no significant immunolabeling of ATP8A2 was observed in the retina of age-matched *Atp8a2*-knockout mice (Fig. 2A). CDC50A labeling was significantly diminished in the outer segment of the knockout mice, but was retained in other retinal layers, probably as a result of its interaction with other P_4-ATPases in the retina. In the retina of the *wl/wl* mice, ATP8A2 was detected, but only in the inner segment of the photoreceptor cells, indicating that mutant ATP8A2 is expressed, but is retained in the endoplasmic reticulum (ER) as an inactive and misfolded protein (Fig. 2B).

Localization of photoreceptor proteins in *Atp8a2*-knockout mice

The effect of ATP8A2 deficiency on the localization of various proteins in photoreceptor cells was examined by immunofluorescence microscopy on retinal cryosections labeled with specific antibodies (Fig. 2C). In WT mice, rhodopsin, which comprises ~80% of the total outer segment membrane protein, is present in both the disc and plasma membrane of rod photoreceptor cells (Molday and Molday, 1987; Papermaster and Dreyer, 1974); the alpha-subunit of the cyclic nucleotide-gated channel (CNGA1) is localized to the plasma membrane of rod outer segments (Cook et al., 1989); and peripherin-2 is distributed along the rim region of rod and cone disc membranes (Molday et al., 1987). These proteins correctly localized to shortened outer segments of the *Atp8a2*-knockout mice. Similarly, other outer segment proteins, including guanylate cyclase 1 (GC1), the ATP binding cassette protein ABCA4, and transducin were also correctly localized to the outer segment layer (data not shown). Cone arrestin used as a cone specific marker also showed normal localization to the shortened cone

Journal of Cell Science (2014) 127, 1138–1149 doi:10.1242/jcs.145052

outer segments of the *Atp8a2*-knockout mice. Furthermore, the localization of various inner segment and synaptic proteins such as GM130 (Golgi), syntaxin 3 (vesicles), Rab11 (endosome), synaptotagmin (synapse), and Na^+/K^+-ATPase were found to be similar to that of WT mice (supplementary material Fig S1). These studies indicate that ATP8A2 deficiency does not impair the selective targeting of photoreceptor proteins to their final destination.

Photoreceptor morphology and degeneration in the retina of *Atp8a2*-knockout and *wl/wl* mice

The morphological characteristics of retinas from *wl/wl* and *Atp8a2*-knockout mice were compared with that of age-matched WT mice to determine the significance of ATP8A2 in photoreceptor structure and survival. At P14, when ATP8A2 is first expressed, the outer nuclear layer and outer segment length of the *wl/wl* mouse retina were indistinguishable from that of WT mice (Fig. 3A). At later ages, the number of photoreceptor nuclei and length of the outer segment were significantly reduced in *wl/wl* mice (Fig. 3A–C). At P30, the *wl/wl* mice showed a 10% reduction in the number of nuclei and the OS length was approximately one-half that of WT mice (11.7±0.3 versus 20.4±0.4 μm). At P60, 30–40% of photoreceptor cells had been lost and the length of the outer segments was one-third of that in WT mice (7±0.3 versus 21.5±0.4 μm). The *Atp8a2*-knockout mouse also showed a decrease in the number of photoreceptors and length of the outer segment layer throughout the eye, with a 15% reduction in outer nuclear layer thickness and 60% reduction (7.7±0.6 versus 18.3±0.9 μm) in outer segment length near the optic nerve at P23 (Fig. 3B).

Next, we examined the ultrastructure of ATP8A2-deficient mouse retina using transmission electron microscopy (Fig. 3C). Despite the reduced length of the outer segments and some disorganization of the outer segments as a result of ongoing photoreceptor degeneration, the morphology of the photoreceptor outer segments was remarkably normal for both the *wl/wl* and knockout mice. The rod disc membrane stacks appeared to be correctly aligned and the structural organization of the hairpin rim region of the rod photoreceptor discs and the adjacent plasma membrane was well preserved. The RPE cells of the Atp8A2-deficient mice showed the presence of some intracellular vesicles not found in the RPE of WT mice, but otherwise the morphological features were similar (see also Fig. 3A,C). The observed vesiculation might be due secondary effects on the RPE cells resulting from the degenerating photoreceptor cells because there is no evidence indicating that ATP8A2 is expressed in RPE cells.

Visual function of photoreceptors

Electroretinograms (ERGs) of the rod-mediated dark-adapted scotopic and cone-mediated light-adapted photopic response were recorded to determine the effect of ATP8A2 deficiency on visual function. Both the *wl/wl* and *Atp8a2*-knockout mice at P30 showed a large reduction in scotopic and photopic response (Fig. 4A,B). The scotopic a- and b-wave amplitudes of the *Atp8a2*-deficient mice were quantified and found to be reduced by 75% and 67%, respectively, compared with values in WT type and heterozygous mice (Fig. 4C,D).

Analysis of rhodopsin and retinal in outer segments of *Atp8a2*-knockout mice

The relative amount of opsin in P23 *Atp8a2*-knockout mice was compared with age-matched WT mice by western blotting. A reduction of 50% was observed for the knockout mice (Fig. 5A). This is generally consistent with the reduction in the length of the outer segments in these mice as observed by microscopy (Figs 2,3). Rhodopsin levels were measured by difference spectrophotometry before and after bleaching. Detergent-solubilized lysates from knockout mice contained 75% lower levels of rhodopsin compared with results in WT mice (Fig. 5B). Rhodopsin content was also determined by retinoid analysis because essentially all the 11-*cis*-retinal is bound to opsin in the dark-adapted mice. A 75% reduction in 11-*cis* retinal was also observed by retinoid analysis. A representative chromatogram is shown in Fig. 5C.

Phospholipid composition

Phospholipid composition was investigated using preparations of hypotonically lysed outer segment membranes from WT and *Atp8a2*-knockout mice containing similar concentrations of opsin and a similar protein profile as analyzed by SDS gel electrophoresis (Fig. 5D). A representative two-dimensional thin layer chromatogram of outer segment lipids is shown in Fig. 5E. Phosphatidylcholine (PC), phosphatidylethanolamine (PE) and phosphatidylserine (PS) constitute the majority of the membrane phospholipids in the outer segments. For WT mice, the composition of these lipids was similar to that previously reported for rat, cow and frog (Boesze-Battaglia et al., 1994; Fliesler and Anderson, 1983; Mason et al., 1973; Poincelot and Abrahamson, 1970). The WT composition of PC:PE:PS was 49±2%:36±2%:15±1% (Fig. 5F). The knockout mouse contained significantly higher levels of PC and lower amounts of PE and PS (66±4%:25±2%:9±2%).

Phagocytosis of outer segments and PS

Exposure of PS on the surface of cells has been associated with phagocytosis in several cell types (Darland-Ransom et al., 2008; Ruggiero et al., 2012). Accordingly, it is possible that the observed shortened outer segments in ATP8A2-deficient mice result from an increase in phagocytosis of outer segments by adjacent RPE cells owing to increased exposure of PS on outer segment surface membranes. To investigate this possibility, we compared the levels of phagocytosis in the *Atp8a2*-knockout mice with WT mice by Toluidine Blue staining for light microscopy (LaVail, 1976). No significant difference in phagocytosis was observed between WT and knockout mice 1 hour after light onset when phagocytosis of outer segments by RPE cells reaches a maximum (Fig. 6A–C). At 6 hours after light onset, phagocytosis was significantly reduced, but no significant difference was observed between the *Atp8a2*-knockout and WT mice. We also measured outer segment phagocytosis in primary cultures of RPE cells isolated from WT mice using an established assay (Gibbs et al., 2003). Phagocytosis of outer segments from *Atp8a2*-knockout mice was lower than that for outer segments from WT mice, but the ratio of outer segments internalized to outer segments bound to the cell surface was the same for both genotypes of mice (Fig. 6D,E).

Fluorescent-labeled annexin V, a protein that specifically binds PS, was used to determine PS exposure on the extracellular side of the plasma membrane of outer segments (Fig. 6F). Annexin V labeled a significant amount of PS exposed on the tips of the outer segments as visualized in whole-mounted retina collected ~1 hour after light onset, in agreement with the finding that PS becomes exposed at the tips of outer segments as a signal for RPE phagocytosis (Ruggiero et al., 2012). However, no significant differences were observed in whole-mounted *Atp8a2*-knockout versus WT retinas (Fig. 6F).

Journal of Cell Science (2014) 127, 1138–1149 doi:10.1242/jcs.145052

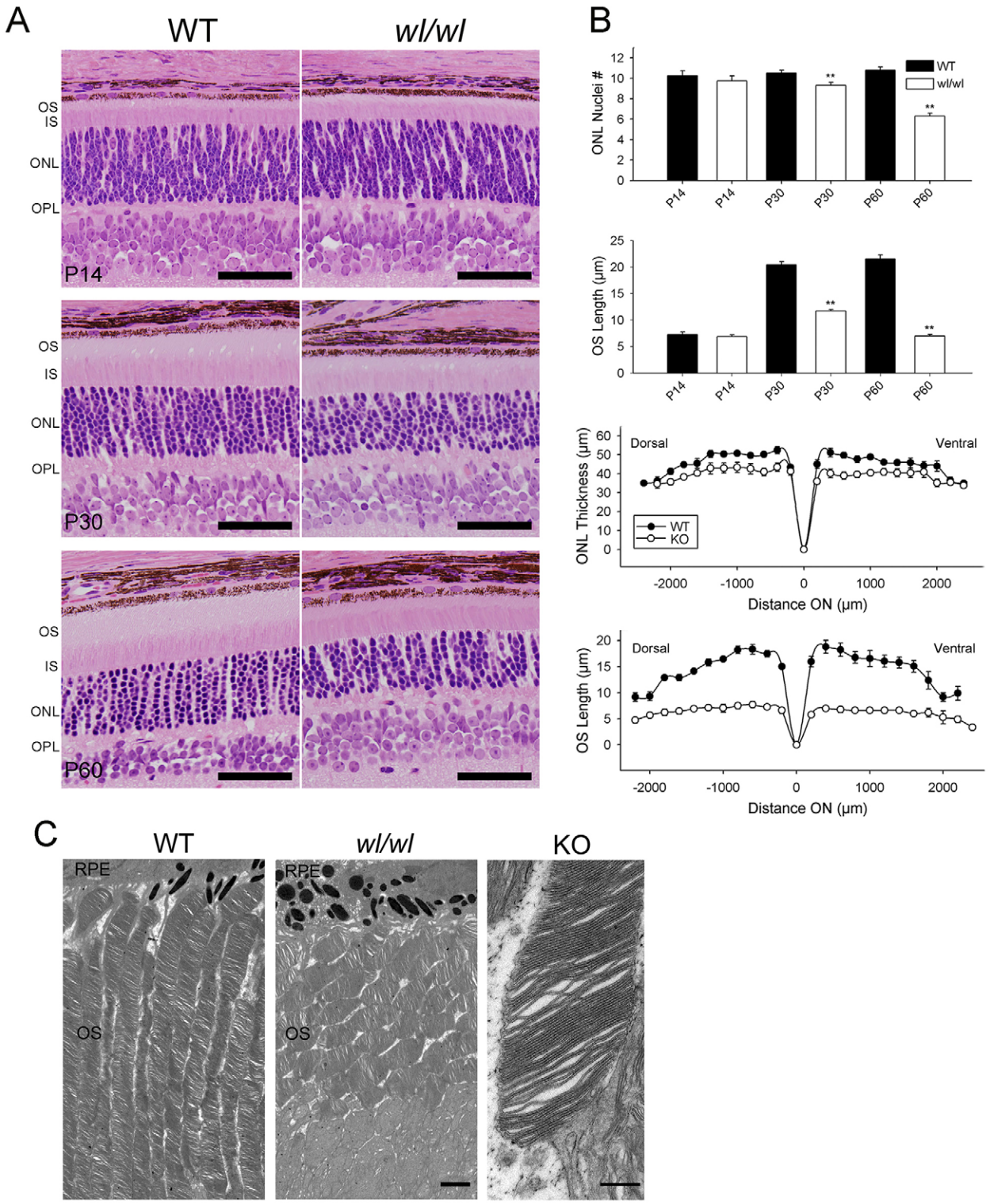

Fig. 3. See next page for legend.

Localization of ATP8A2 to the Golgi and endosomes in photoreceptors and PC12 cells

Because removal of the tips of the outer segments by phagocytosis appears normal in the *Atp8a2*-knockout mouse, we considered the possibility that ATP8A2 plays a role in outer segment morphogenesis by vesicle trafficking within the inner segment of photoreceptor cells. To explore this possibility, we examined in more detail the localization of ATP8A2 in photoreceptor cells of WT mice by confocal scanning microscopy. Immunofluorescence labeling of ATP8A2 was seen just above the ONL which partially colocalized with the Golgi marker GM130 (Fig. 7A) indicating that a fraction of ATP8A2 resides in or very close to the Golgi complex of photoreceptors.

We further examined the distribution of ATP8A2 in transfected and differentiated PC12 cells, which exhibit long neuron-like

Journal of Cell Science (2014) 127, 1138–1149 doi:10.1242/jcs.145052

Fig. 3. Effect of ATP8A2 deficiency on photoreceptor survival, morphology and outer segment structure. (A) The morphology of the *wl/wl* retina is indistinguishable from that of control wild-type mice at 2 weeks of age (P14; top panels) by light microscopy. Outer segments are shorter at one (P30; middle panels) and two (P60; bottom panels) months of age. The number of photoreceptor nuclei is reduced in *wl/wl* mice at P30 and P60. OS, outer segment; IS, inner segment; ONL, outer nuclear layer; OPL, outer plexiform layer. (B) The number of photoreceptor nuclei in the outer nuclear layer (ONL) and the outer segment (OS) length in wild-type (WT), *wl/wl* and knockout mice. At 1 month (P30), the number of nuclei in the ONL was reduced from 10 rows in wild-type to 9 rows in the *wl/wl* mice (top panel). At 2 months (P60), the number of rows of nuclei in the ONL was reduced to 6–7 rows. At P30, the outer segment (OS) length of *wl/wl* mice was ~50% of WT mice (second panel). At P60, the OS length was further reduced to approximately one-third of WT mice (n=4). The thickness of the ONL (top) and OS length (bottom) for 23-day-old WT and knockout mice plotted as a function of distance from the optic nerve (ON) (wild-type, n=6; knockout, n=7) (third and bottom panel). $^{**}P<0.05$ between the WT and *wl/wl* mice. Error bars represent s.e. (C). Ultrastructural analysis of photoreceptor outer segments from *wl/wl* and knockout retina adjacent to the retinal pigment epithelial (RPE) cells by electron microscopy. At 6 weeks, outer segments of the *wl/wl* mice (middle panel) are shorter than outer segments from wild-type mice (left panel) and show some disorganization in the arrangement of outer segments as a result of photoreceptor degeneration. However, the ultrastructure of the outer segments appeared normal. The ultrastructure of a rod outer segment from a 30-day-old knockout mouse at higher magnification appears normal despite the shorter length. Scale bars: 50 µm (A), 2 µm (C, right and middle panels), 0.5 µm (C, left panel).

axons and dendrites (neurites). In agreement with a recent report (Xu et al., 2012), co-transfection of NGF-differentiated PC12 cells with ATP8A2 and CDC50A promoted neurite outgrowth (94±7 versus 62±5 µm). A large fraction of the expressed ATP8A2 was found to reside within the Golgi complex and at the tips of the neurites (Fig. 7B). ATP8A2 colocalized with CDC50A (data not shown) and Rab11, indicating that the ATP8A2–CDC50A complex is present in endosomes as well as the trans-Golgi network (Fig. 7B).

Auditory brainstem response

In addition to the visual system, we assessed hearing in *wl/wl* mice. Homozygous mutant *wl/wl* mice on a C57BL/6J (B6) strain background exhibited a diminished auditory startle response. Therefore, we used auditory brainstem response (ABR) threshold measurements to assess hearing in *wl/wl* mice. Analysis of representative ABR recordings revealed that the ABR threshold of mutant mice was much higher than that of control animals (Fig. 8A,B). At 2 months of age, the 16 kHz ABR thresholds of *wl/wl* mice were on average 37 dB higher than that of WT (Fig. 8C).

To understand the basis of this auditory defect, we analyzed the inner ear morphology of the *wl/wl* mice by light microscopy. Cross sections through the basal turns of cochleae showed that although the overall structure of the organ of Corti appeared normal and the outer and inner hair cells were intact (Fig. 8F,G), a substantial number of the spiral ganglion cells had been lost (21±2 versus 7±2; n=4) in 2-month-old *wl/wl* mice (Fig. 8D,E).

DISCUSSION

In this study we have analyzed two lines of mice deficient in ATP8A2-catalyzed phospholipid transport. The phenotype of the newly generated *Atp8a2*-knockout mouse was similar to the *wl/wl* mouse, which harbors a deletion of 7 highly conserved amino acids (TAIEDRL) in the nucleotide-binding domain of ATP8A2 (Zhu et al., 2012). Both mice were smaller than their littermates, walked with an abnormal gait, survived for only 2 months and exhibited similar aberrations in the visual system.

A prominent feature of ATP8A2-deficient mice is the progressive reduction in the length of the retinal photoreceptor outer segments, with no detectable abnormality in their ultrastructural organization. Outer segments are dynamic structures which turnover every 10 days (LaVail, 1976; Sung and Chuang, 2010). Adjacent RPE cells engulf the distal tenth of

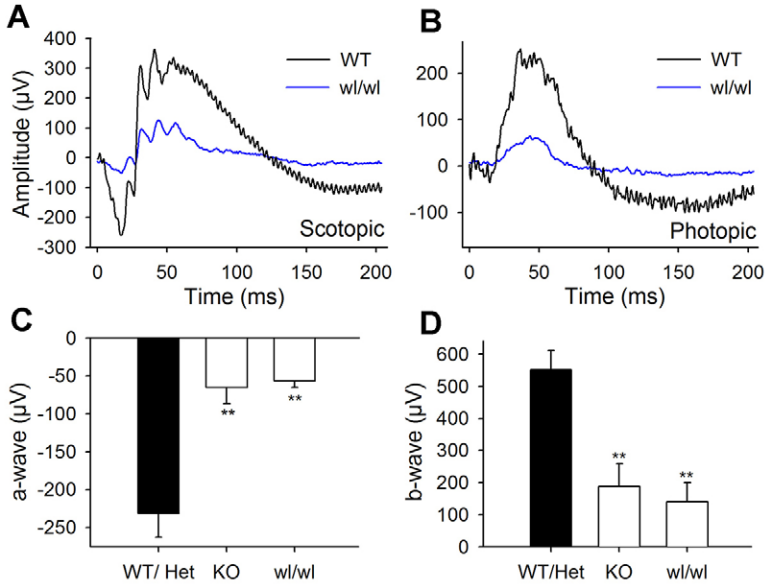

Fig. 4. Effect of ATP8A2 deficiency on visual function as measured by electroretinograms (ERGs). Representative traces of (A) rod (scotopic) and (B) cone (photopic) ERG for 1-month-old WT (black line) and *wl/wl* (blue line) mice. Quantification of (C) scotopic a-wave and (D) b-wave amplitudes for WT and heterozygous (Het) (n=9), knockout (n=6) and *wl/wl* mice (n=4). The a- and b- waves are markedly smaller in the mutant mice. $^{**}P<0.05$ between WT and knockout or *wl/wl* mice. Error values represent s.e.

Journal of Cell Science (2014) 127, 1138–1149 doi:10.1242/jcs.145052

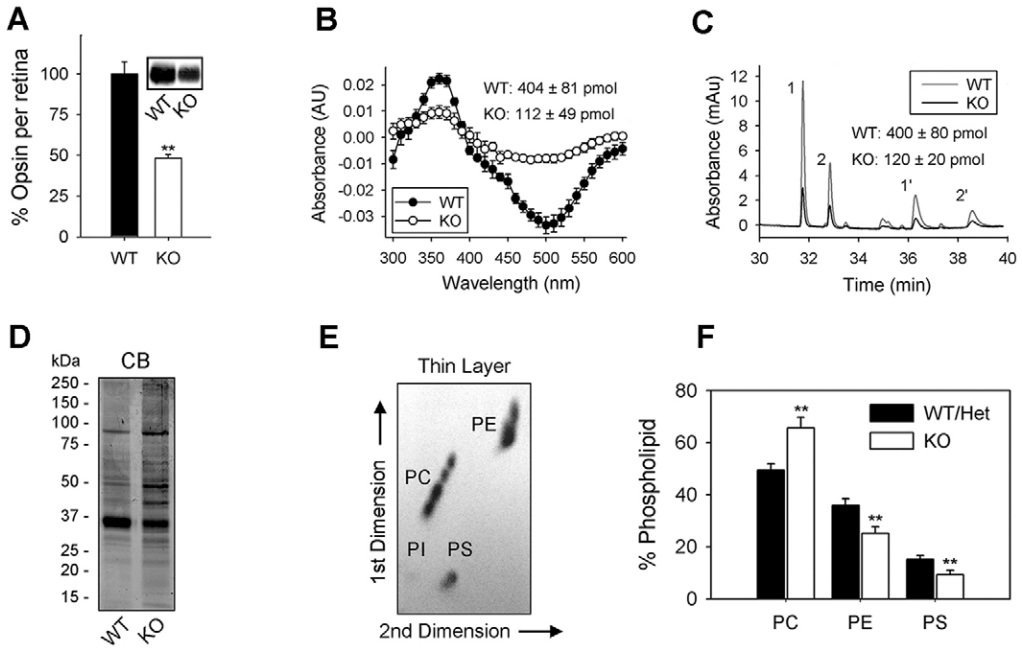

Fig. 5. Quantification of opsin, rhodopsin, 11-*cis* retinal and phospholipids in *Atp8a2*-knockout mice. (A) The amount of opsin in detergent-solubilized lysates from retinas of wild-type (WT) and knockout (KO) mice at 23 days of age was detected and quantified on western blots. The relative quantification of opsin per retina is shown (WT, $n=6$; knockout, $n=4$). Insert shows a representative western blot of opsin. (B) Difference spectrum calculated from spectra measured before and after rhodopsin bleaching for WT (closed circles) and knockout (open circles) at 23 days of age (WT, $n=8$; knockout, $n=6$). (C) Chromatographic separation of retinoids from WT (gray) and knockout (black) eyes. Retinoids were extracted from the eye and separated by normal phase high performance liquid chromatography. A representative chromatogram is shown. 1 and 1′ represent syn- and anti-11-cis retinal oximes and 2 and 2′ represent the syn- and anti-all-trans retinal oximes. Quantification of 11-cis-retinal is given (WT, $n=10$; knockout, $n=6$). (D) Coomassie Blue (CB)-stained SDS gel of isolated outer segment discs from WT and knockout mice. (E) Representative thin layer chromatograph of outer segment lipids stained with I_2. PC, phosphatidylcholine PE, phosphatidylethanolamine; PI, phosphatidylinositol; PS, phosphatidylserine. (F) Lipid composition in wild-type (WT/Het) and knockout (KO) outer segments determined by phosphate analysis (WT, $n=13$; knockout, $n=5$). $^{**}P<0.05$ between the WT and knockout mice.

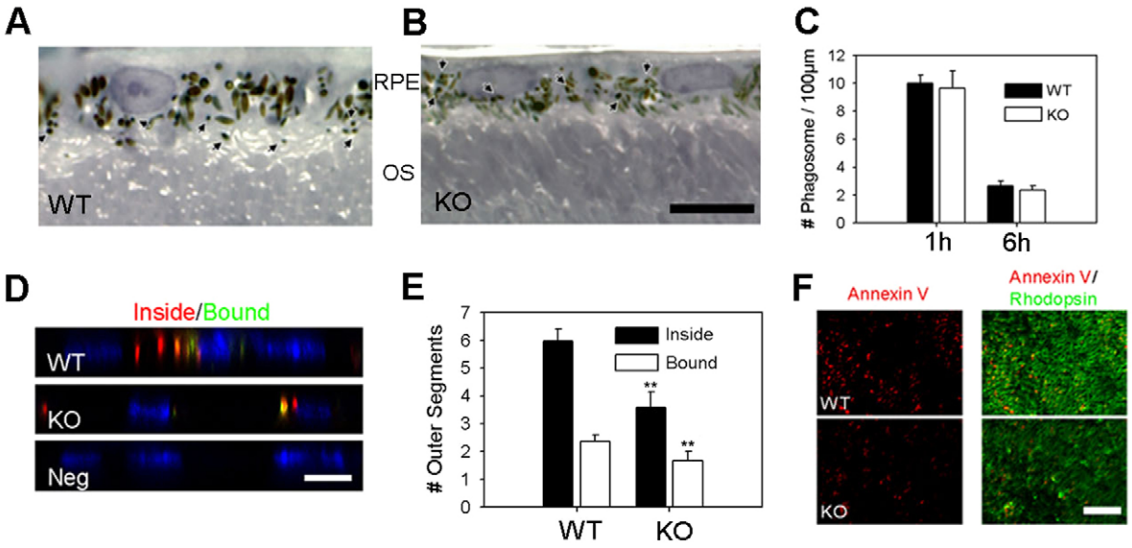

Fig. 6. Phagocytosis and annexin V binding to photoreceptor outer segments in *Atp8a2*-knockout mice. Toluidine Blue staining of retinas isolated 1 hour after light onset for (A) WT and (B) *Atp8a2*-knockout retinas. Phagosomes can be seen in retinal pigment epithelium (RPE) layer as indicated (arrows). (C) Quantification of phagosomes 1 hour and 6 hours after light onset. There is no significant difference in phagocytosis between the WT and knockout mice ($n=3$). (D) Outer segments were added to polarized RPE primary cultures. Bound (green) and internalized (red) outer segments were visualized using the Rho 4D2 antibody against rhodopsin. Nuclei (blue) are stained with DAPI. For a negative control, no outer segments were added. (E) Quantification of bound and internalized outer segments in RPE primary cultures. Significantly fewer knockout outer segments are evident in RPE cells ($n=3$). $^{**}P<0.05$ between WT and knockout mice. Error values represent s.e. (F) Annexin V labeling (red) of photoreceptor outer segments in retina whole mounts prepared 1 hour after light onset. Retinas were also labeled with the Rho 4D2 antibody (green), a rhodopsin antibody that labels the extracellular surface of rod outer segments. Photoreceptor outer segments are directed toward the viewer. No significant difference in annexin V binding to PS on rod outer segments in the retina of WT and knockout mice was found. Scale bars: 10 µm.

Journal of Cell Science (2014) 127, 1138–1149 doi:10.1242/jcs.145052

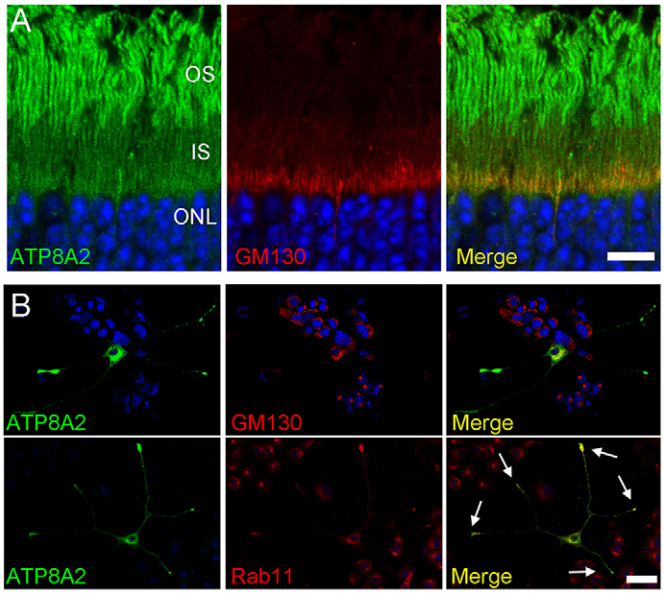

Fig. 7. Localization of ATP8A2 to the Golgi and endosomes of photoreceptor inner segments and PC12 cells by immunofluorescence microscopy. (A) Photoreceptors in retina cryosections of WT mice were labeled with a polyclonal antibody against ATP8A2 (green) and a monoclonal antibody against the Golgi marker GM130 (red) and counterstained with 4′,6-diamidino-2-phenylindole (blue). The merged image shows partial colocalization of ATP8A2 and GM130 (yellow). OS, outer segments; IS, inner segments; ONL, outer nuclear layer. (B) ATP8A2 (green) expressed in PC12 cells partially colocalizes (yellow) with GM130 and Rab11 (red). Arrows indicate the neurite tips. Scale bars: 10 μm (A), 50 μm (B).

an outer segment every 24 hours. This is compensated by the addition of newly synthesized membrane at the proximal end of the outer segment via vesicle trafficking from the inner segment. The balance between phagocytosis and disc morphogenesis maintains a constant length of the outer segment. We reasoned that the progressive reduction in outer segment length in the ATP8A2-deficient mice might result from either an increase in phagocytosis or a decrease in outer segment morphogenesis. Because increased exposure of PS on the extracellular surface of cells has been implicated in the recognition step for a number of phagocytic processes (Ruggiero et al., 2012; Wu et al., 2006), we first investigated whether *Atp8a2*-knockout mice showed an increase in PS on the surface of outer segments and higher levels of phagosomes in RPE cells. However, annexin V labeling of outer segments and the number of phagosomes in the knockout and WT mouse were similar, indicating that ATP8A2 deficiency does not directly affect PS cell surface exposure or phagocytosis by RPE cells. Other mechanisms appear to control PS exposure on the outer segment plasma membrane as part of the phagocytic process.

The shortened outer segments in ATP8A2-deficient mice more likely arise from decreased vesicle trafficking to the outer segment required for disc morphogenesis. A number of studies have implicated ATP8A2 and related P_4-ATPases in protein-mediated vesicle trafficking. Overexpression of ATP8A2 and CDC50A increases the length of neurite outgrowths in NGF-differentiated PC12 cells and primary cultures of rat hippocampal neurons, whereas depletion of ATP8A2 or CDC50A reduces neurite length (Xu et al., 2012). In this study, we have confirmed that overexpression of the ATP8A2–CDC50A complex increases

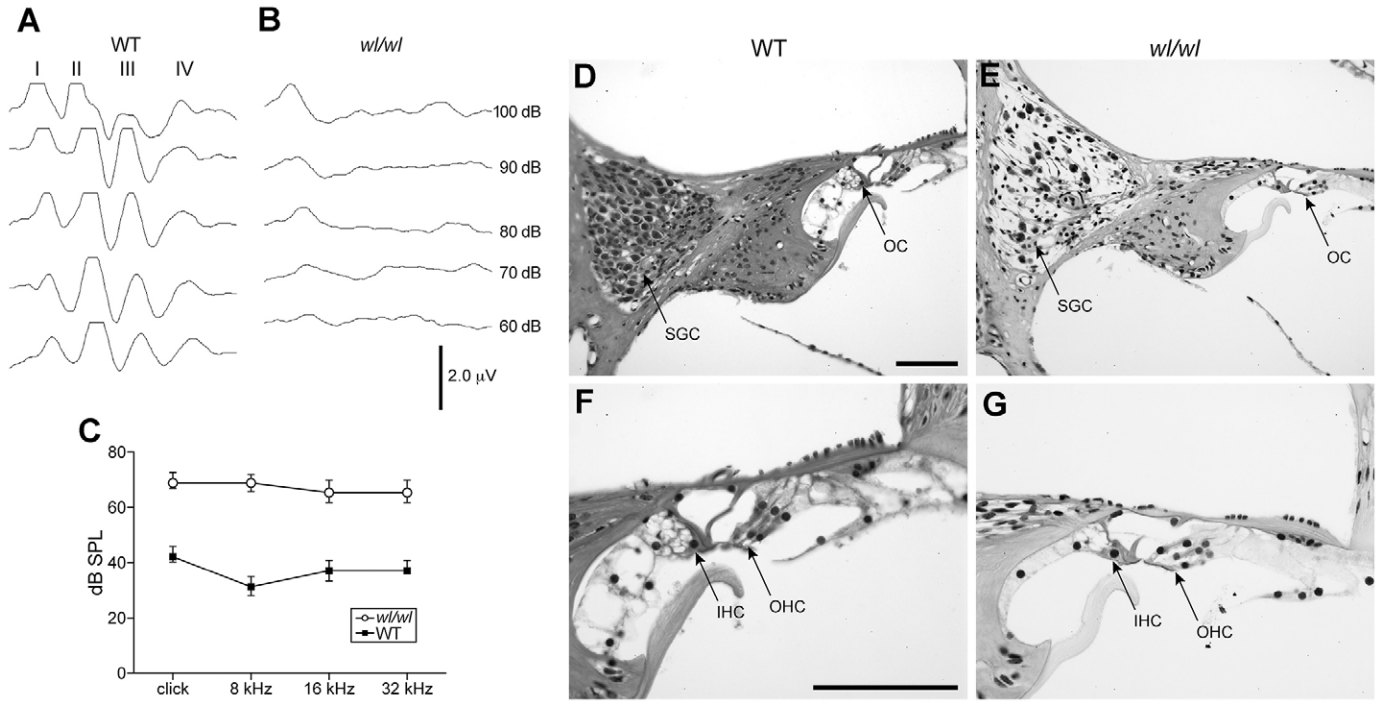

Fig. 8. Deafness and cochlear pathology of *wl/wl* mutant mice. Representative trace of ABR recording for (A) WT and (B) *wl/wl* mice using 16 kHz stimulus frequencies at P50. Note the lack of typical ABR peaks in *wl/wl* mutant animals. (C) ABR thresholds (dB SPL) of *wl/wl* mutant mice and non-mutant controls tested at 35–63 days of age (n=4). Error bars represent s.d. of the threshold means. (D–G) Cross sections through the basal turn of the cochlea from a normal heterozygous mouse (D,F) and a *wl/wl* mutant mouse (E,G) examined at 2 months of age. Note the decreased density of spiral ganglion cells (SGC) in the *wl/wl* cochlea. Outer hair cells and inner hair cells appear normal. SGC, spiral ganglion cell; OC, organ of Corti; IHC, inner hair cells; OHC, outer hair cells. Scale bars: 100 μm.

Journal of Cell Science (2014) 127, 1138–1149 doi:10.1242/jcs.145052

neurite length in PC12 cells and have further shown that this complex localizes to the Golgi complex and endosomes, as well as the tips of the neurites of transfected PC12 cells. Drs2p, the yeast ortholog of ATP8A2, is a key regulator of the vesicle budding from the trans-Golgi network (Sebastian et al., 2012). ArfGEF binds to Drs2p and stimulates its lipid flippase activity. ArfGEFs recruit activated Arf proteins and phospholipid flipping drives vesicle bud formation. Activated Arf proteins recruit adaptors and coat proteins. We have shown here the existence of a population of ATP8A2 in the inner segment of photoreceptor cells with a significant fraction colocalizing with the Golgi marker GM130, in agreement with ATP8A2 localization in transfected PC12 cells and other cells (Coleman and Molday, 2011; van der Velden et al., 2010). On the basis of these studies, we propose that the reduction in outer segment length observed in the *Atp8a2* mutant mice is due to a decrease in vesicle budding and trafficking in the inner segment required for efficient disc morphogenesis. The fact that outer segments are formed in these mutant mice suggests that another P_4-ATPase, probably ATP8A1, partially compensates for the loss of ATP8A2 within the inner segment, allowing vesicle budding and trafficking to occur in ATP8A2-deficient mice, but less efficiently, thereby giving rise to shortened outer segments. Photoreceptor degeneration observed in the ATP8A2-deficient mice is most likely a consequence of a reduction in outer segment formation because it has been shown previously that genetic defects that affect normal outer segment morphogenesis result in photoreceptor degeneration (Hawkins et al., 1985; Humphries et al., 1997). ATP8A2-mediated vesicle budding and trafficking also appears to be directly involved in neurite outgrowth in PC12 and hippocampal cells. Axonal degeneration observed in *wl/wl* mice deficient in ATP8A2 might also result from defective vesicle trafficking (Zhu et al., 2012).

Another feature of ATP8A2-deficient mice is the marked loss in visual function as measured by the ERGs. The 50% reduction in outer segment length could contribute to the observed decrease in a-wave amplitude of the ERG response, but this is likely to be a relatively small contribution. Heterozygous rhodopsin-knockout mice with an outer segment length and volume that were 60% and 40%, respectively, that of WT mice, show only a 15% reduction in the a-wave amplitude (Liang et al., 2004). Instead, the large reduction in the photoresponse observed in ATP8A2-deficient mice might be due to the altered lipid environment experienced by opsin and other membrane-associated proteins, which in turn impacts phototransduction. It is not known why the absence of ATP8A2 alters the lipid composition of the outer segment. One possibility is that ATP8A2 in the Golgi and endosomes concentrates PS and PE in budding vesicles through bilayer coupling resulting in higher PS or PE levels in the transport vesicles destined for the outer segment. Accordingly, in the absence of ATP8A2, a lower level of these lipids would be present in the outer segments of the *Atp8a2*-knockout mouse. Another possibility is that the biosynthesis of these lipids is downregulated to compensate for the absence of the transporter to maintain their membrane distribution. Finally, it cannot be ruled out that the difference in phospholipid contents arises from membrane contaminants in the outer segment preparation of the knockout mice, although analysis of the protein content by SDS gel electrophoresis does not reveal significant differences in protein content between outer segments of WT and knockout mice. Interestingly, a reduction in PS and PE composition has been previously reported for yeast lacking the P4-ATPase Drs2p (Pomorski et al., 2003). It remains to be determined whether alteration of phospholipid composition is a common feature of biological systems displaying a deficiency in other P4-ATPases, or if this alteration is specific for ATP8A2 and Drs2p deficiency.

Interestingly, this change in lipid composition does not affect the morphological features of photoreceptor outer segments, but does affect rhodopsin content. A decrease in opsin content of 50% in 1-month-old *Atp8a2*-knockout mice is expected on the basis of the 50% reduction in outer segment length. However, rhodopsin content as measured by spectral bleaching and retinoid analysis is only 25% of the WT value, indicating that only 50% of the opsin contains a bound 11-*cis* retinal chromophore. This suggests that either a portion of opsin is misfolded, preventing the binding of 11-*cis* retinal or the supply of 11-*cis* retinal to outer segments is impaired. Rhodopsin activation has been reported to be highly dependent on membrane environment with meta II rhodopsin being formed more readily in the presence of PE and PS (Gibson and Brown, 1991). Helix 8 of rhodopsin acts as a membrane switch, causing adoption of a helical conformation upon PS binding (Krishna et al., 2002). Helix 8 has also been shown to be important for protein folding, binding of 11-*cis* retinal and transducin activation (Natochin et al., 2003). Accordingly, the significant reduction in the a-wave amplitude of the ERGs observed in *Atp8a2*-deficient mice might result from the effect of altered phospholipid composition on phototransduction.

A principal function of ATP8A2 is to actively transport aminophospholipids across the lipid bilayer to generate phospholipid asymmetry in biological membranes. Because ATP8A2 is present in outer segment disc membranes, it might be expected to induce aminophospholipid asymmetry. A number of earlier studies have focused on phospholipid asymmetry in bovine photoreceptor disc membranes. Although initial reports suggested that disc membranes were highly asymmetrical with respect to the transbilayer distribution of PS and PE in disc membranes (Miljanich et al., 1981; Wu and Hubbell, 1993), subsequent studies have indicated that PC and PE are symmetrically distributed across the bilayer with PS exhibiting an ATP-independent asymmetrical distribution resulting from the high density and orientation of rhodopsin (Hessel et al., 2000; Wu and Hubbell, 1993). The recently reported scramblase activity of rhodopsin (Menon et al., 2011) might overwhelm the ATP-dependent phospholipid flippase activity of ATP8A2, resulting in a random distribution of phospholipids across the disc membrane. Although the ATP8A2 phospholipid transport activity might not play an important role in establishing the bulk phospholipid transbilayer distribution, it could play a role in generating transient local aminophospholipid asymmetry in discs, which is important for phototransduction. It remains to be determined whether localization of ATP8A2 to the tips of the neurite outgrowth and possibly synaptic vesicles (as observed in PC12 cells) plays an important role in the generation of phospholipid asymmetry and neuronal function.

In addition to affecting visual function, ATP8A2 deficiency was found to cause a loss in hearing and degeneration of cochlea spiral ganglion cells. This is the second P_4-ATPase associated with hearing deficiency. Previously, it was reported that deficiency in functional ATP8B1 in humans and mutant mice causes hearing loss, associated with progressive degeneration of cochlear hair cells consistent with the localization of ATP8B1 in the sterocilia of hair cells (Stapelbroek et al., 2009). These combined studies highlight the crucial roles played by distinct P4-ATPases in different auditory cells. The mechanism by which deficiency of ATP8A2 causes loss in auditory function and

Journal of Cell Science (2014) 127, 1138–1149 doi:10.1242/jcs.145052

neuronal degeneration remains to be determined. It is possible that these phospholipid transporters are important in generating and maintaining PS asymmetry required for neuronal vesicle trafficking and auditory function.

Recently, a missense mutation (I376M), which abolishes ATP8A2 phosphatidylserine flippase activity (our unpublished data) in a highly conserved transmembrane segment of ATP8A2 has been reported in several members of a consanguineous family from Turkey (Emre et al., 2012). Affected individuals displayed severe neurological complications including mental retardation, mild cerebellar and cerebral atrophy and truncal ataxia. Unfortunately, members of this family declined neuro-ophthalmological examinations and hence the effect of ATP8A2 deficiency in the human visual and auditory sensory systems could not be determined.

In summary, our studies indicate that the ATP8A2–CDC50A phospholipid transporter plays a crucial role in the function and survival of photoreceptors and spiral ganglion cells and implicate ATP8A2 as a crucial mediator of vesicle trafficking in neuronal cells.

MATERIALS AND METHODS

Experimental animals

All animal protocols were approved by the Animal Care Committee of the University of British Columbia and conform to the Canadian Council on Animal Care guidelines. Mice were raised in cyclic lighting conditions with a 12 hour light and 12 hour dark cycle. The Association for Assessment and Accreditation of Laboratory Animal Care guidelines was followed for all animal procedures at the Jackson Laboratory and procedures were approved by the Institutional Animal Care and Use Committee of the Jackson Laboratory.

Knockout mice were produced by InGenious Targeting Laboratory (Stony Brook, NY). An 11.6 kb fragment spanning exons 10–16 used to construct the targeting vector was first subcloned from a positively identified C57BL/6 BAC clone into the pSP72 vector (Promega, Madison, WI). The neomycin resistance cassette replaced 3.86 kb of the gene including exons 11–13. This targeting vector was linearized by *Not*I and transfected by electroporation of C57BL/6 × 129/SvEv hybrid embryonic stem cells. Homologously recombined clones were selected by neomycin, screened by PCR and confirmed by Southern blotting. Targeted stem cells were microinjected into C57BL/6 blastocysts. Resulting chimeras were mated to WT C57BL/6 mice to generate F1 heterozygous offspring. Heterozygous mice were crossed and matings producing homozygous *wl/wl* mutants or knockout were kept for strain production. Thus, the knockout mice had a mixed 129SvEv and C57BL/6 background.

The *wl* mutation backcrossed to strain C57BL/6J was used (Zhu et al., 2012). As standard practice for *wl/wl* mutant mice, dry food was supplemented with a soft maintenance diet (DietGel 76A, ClearH_2O, Portland, ME). Knockout mice were provided with dry food at the bottom of the cage.

Genotyping by PCR

Genomic DNA extracted from ear punches was amplified by PCR using primers for the *Atp8a2* gene (forward, 5′-ATGCAGGGTCTGTGAGT-AGTAGTC-3′) and (reverse, 5′-GTGGCCAGATGACAAGCATTCC-CT-3′) and the neomycin resistance cassette (reverse, 5′-TGCGAGG-CCAGAGGCCACTTGTGTAGC-3′). Amplification was performed using the REDExtract-N-Amp kit (Sigma) with the addition of 0.5 M Betaine (Sigma, Oakville, ON). The first cycle used 94℃ for 3 minutes, followed by 35 cycles of 94℃ for 30 seconds, 60℃ for 30 seconds and 72℃ for 1.5 minutes. To identify mice with the *wl* allele, the following primers were used: forward, 5′-TGAACTGTCCCTTAACTGATGGTA-3′ and reverse, 5′-TGGCTATGGTTTCTGGAACG-3′. This primer pair spans the 21 base-pair deletion in exon 22 in *wl* allele and produces a 108 bp amplicon in WT controls and an 87 bp amplicon in *wl/wl* mice.

Transmission electron microscopy and light microscopy

Eyes were fixed in 1% glutaraldehyde and 1% paraformaldehyde in phosphate buffer at 4℃ for ∼1 week. Retinas were treated with OsO_4 for 1 hour at a concentration of 40 mM in 0.1 M cacodylate buffer pH 7.4 containing 0.2% sucrose. Samples were dehydrated with ethanol and embedded in Epon 812-Araldite resin. Ultrathin sections (0.07 µm) were cut and stained with uranyl acetate and lead citrate solution. For light microscopy, thin sections (0.5 µm) were cut and stained with Toluidine Blue. Blue particles ≤1 µm were counted as phagosomes. For hematoxylin and eosin staining (H&E), eyes were fixed overnight in 1.22% glutaraldehyde and 0.8% paraformaldehyde in 0.08 M phosphate buffer, embedded in Technovit resin, cut in 1.5 µm sections. For cochlear tissue, anesthetized mice were perfused with PBS followed by 4% paraformaldehyde. Tissues were decalcified with Cal-EX solution for 24 hours, and embedded in paraffin. 5 µm sections were counterstained in H&E. Spiral ganglion cells were counted in an 80×80 µm square positioned over the center of the cochlear ganglion.

RT-PCR

RNA was extracted from retinas using the RNeasy kit (Qiagen, Maryland, MA). Genomic DNA was removed by incubation of 2 µg of total RNA with 2 units DNaseI for 30 minutes at 37℃. Complementary DNA was prepared by reverse transcription of 1 µg of total RNA using the iScript cDNA Synthesis kit (Bio-Rad). Amplification of the cDNA was performed with the following primers specific to *Atp8a2*: forward, 5′-ACGAGGGACGTGCTCATGAAGC-3′ and reverse, 5′-CCTCAAGTG-TCACCAGCAGGCT-3′; and for glyceraldehyde phosphate dehydrogenase (*Gapdh*): forward, 5′-ATCAAATGGGGTGAGGCCGGTG-3′ and reverse, 5′-CGGCATCGAAGGTGGAAGAGTG-3′. PCR was performed using *Taq* (New England Biolabs, Ipswich, MA) for 30 cycles for *Atp8a2* and 25 cycles for *Gapdh* and the PCR products were visualized on 1.5% agarose gels.

Electroretinograms

Animals were kept in the dark for at least 2 hours before the experiment and anesthetized with an intraperitoneal injection of xylazine (7 mg/g body weight) and ketamine (15 mg/g body weight) in PBS. A heated water blanket was used to keep animal body temperature constant at 38℃. For ERG evaluation of mice, an Espion Visual Electrophysiology System (Diagnosys, Westford, MA) was used. Scotopic recordings used an intensity setting of 1.42 log scotopic troland. Photopic recordings were performed using an intensity setting of 1.13 log photopic troland.

Preparation of photoreceptor outer segments

Purified mouse photoreceptor outer segments were prepared according to the Optiprep method (Tsang et al., 1998). Briefly, 12 mouse retinas were vortexed for 1 minute in 120 µl of Ringer's buffer (10 mM HEPES, pH 7.4, 130 mM NaCl, 3.6 mM KCl, 2.4 mM $MgCl_2$, 1.2 mM $CaCl_2$ and 0.02 mM EDTA) containing 8% Optiprep (Sigma, Oakville, ON) and complete inhibitor (Roche, Laval, QU). The retinas were centrifuged at 200 ***g*** for 1 minute, the supernatant was collected, and the procedure was repeated five times. The supernatant was overlaid on a 10% and 18% Optiprep step gradient in Ringer's buffer and centrifuged for 30 minutes at 26,500 ***g***. The outer segment membranes were collected on top of the 18% Optiprep with a needle, diluted with six volumes of Ringer's buffer, and centrifuged at 26,500 ***g*** for 30 minutes. The pellet was resuspended in Ringers buffer containing 8% Optiprep and complete inhibitor and stored at −30℃. Bovine outer segments were isolated as described (Papermaster and Dreyer, 1974).

Polyclonal ATP8A2 antibody

A DNA fragment corresponding to amino acids 369–644 of mouse ATP8A2 (NM_016529.4) was cloned in-frame with glutathione S-transferase (GST) in the pGEX-4T-1 vector using the *Eco*RI and *Xho*I restriction sites. This fragment was subcloned into pMAL-c2 using *Eco*RI and *Sal*I in-frame with maltose binding protein (MBP). ATP8A2 antibodies were raised in rabbits immunized seven times with 500 µg of the GST-fusion protein (YenZym Antibodies, Burlingame, CA). ATP8A2-specific antibodies were purified from 50 ml of serum in PBS on an affinity column consisting of MBP-fusion protein coupled to Sepharose 2B by CNBr and eluted with 0.1 M glycine (pH 2.5).

Journal of Cell Science (2014) 127, 1138–1149 doi:10.1242/jcs.145052

Western blotting

Proteins were separated on 9% polyacrylamide SDS gels and stained with Coomassie Blue or transferred to Immobilon FL membranes (Millipore, Bedford, MA) in buffer containing 25 mM Tris-HCl, pH 8.3, 192 mM glycine, 10% methanol. Membranes were blocked with 1% milk in PBS for 30 minutes. Primary antibody cell culture supernatants were diluted in PBS and 0.1% milk at the following concentrations: Atp6C11 (1:10), Cdc50-7F4 (1:10), 3F4 (1:20), 1D1 (1:20), 5H2 (1:10), and 1D4 (1:1000). The ATP8A2 polyclonal and the β-actin polyclonal (ab8227, Abcam) antibodies were diluted at a concentration of 0.3 µg/ml and 0.2 µg/ml respectively. Blots were incubated with primary antibodies for 40 minutes, washed with PBS containing 0.05% Tween 20 (PBST), incubated for 40 minutes with secondary antibody (goat anti-mouse or anti-rabbit conjugated with IR dye 680 or 800 (LI-COR, Lincoln, NE) diluted 1:20,000 in PBST containing 0.5% milk, and washed with PBST prior to visualization on a LI-COR Odyssey imager (LI-COR, Lincoln, NE).

Immunofluorescence microscopy

Cryosections of mouse retinas were prepared by fixing eyes in 4% paraformaldehyde, 100 mM phosphate buffer (PB) (pH 7.4) for 1–3 hours as previously described (Cheng et al., 2013). Cryosections were cut using a cryostat at a thickness of 10 µm. Labeling with various antibodies was performed as previously described (Cheng et al., 2013; Coleman et al., 2009; Coleman and Molday, 2011; Kwok et al., 2008). PC12 cells were cultured and differentiated according to (Xu et al., 2012). Sections were blocked and permeabilized with 10% normal goat serum and 0.2% Triton X-100 in phosphate buffer for 30 minutes. Labeling of primary antibodies was carried out overnight at room temperature or in the case of opsin Rho-1D4 labeling, for 1 hour. Primary antibodies (cell culture supernatant and purified antibodies) were diluted in phosphate buffer containing 2.5% normal goat serum and 0.1% Triton X-100 at the following concentrations: ATP8A2 polyclonal antibody (purified 0.3 µg/ml), Cdc50-7F4 monoclonal antibody (supernatant 1:2), Per5H2 monoclonal antibody to peripherin-2 (supernatant 1:10), PMc 1D1 monoclonal antibody to CNGA1 channel subunit (supernatant 1:20), Rho1D4 monoclonal antibody to rhodopsin (supernatant 1:1000), Rho 4D2 monoclonal antibody to rhodopsin (supernatant 1:100), cone arrestin polyclonal antibody (purified 0.5 µg/ml, AB15282, Millipore, Bedford, MA), GM130 monoclonal monoclonal antibody (2.5 µg/ml, 61-0822, BD Biosciences, Mississauga, ON) and Rab11 monoclonal antibody (2.5 µg/ml, 610656, BD Biosciences, Mississauga, ON). Sections were washed with PB and labeled for 1 hour with Alexa-Fluor-488- or Alex-Fluor-594-labeled goat anti-mouse or anti-rabbit Ig secondary antibody (diluted 1:1000) and counterstained with DAPI.

Retinal whole mounts were prepared as previously described (Cheng et al., 2013). Briefly, mouse eyes were lightly fixed for 1 hour after light onset with 4% paraformaldehyde for 15 minutes. The retina was dissected from the retinal pigment epithelial layer and fixed for another 15 minutes. After washing in 10 mM HEPES, pH 7.4, 140 mM NaCl and 2.5 mM $CaCl_2$, the retinas were labeled with annexin-V–Alex-Fluor-594 (Molecular Probes, Eugene, OR) for 1 hour in 10 mM HEPES, pH 7.4, 140 mM NaCl, 2.5 mM $CaCl_2$. The retinas were then washed and relabeled with the Rho 4D2 antibody (supernatant 1:100). The Rho 4D2 antibody is against the N-terminus of rhodopsin and labels rhodopsin exposed on the extracellular surface of rod outer segments without permeabilization (Hicks and Molday, 1986; Laird and Molday, 1988). After labeling with the secondary antibody, the retinas were mounted on slides with the photoreceptor outer segments facing up and visualized on a Zeiss LSM 700 confocal scanning microscope.

Measurement of outer nuclear layer and outer segment layers

Eyes from WT or knockout mice were removed, marked on the nasal side for orientation, cut into cryosections, and labeled with DAPI and the Rho1D4 antibody as described above. The outer nuclear layer and outer segment layers were defined by DAPI and Rho1D4 labeling, respectively. Three measurements of the outer nuclear layer and outer segment layers were taken every 200 µm from the optic nerve and averaged. The optic nerve was defined as 0 µm. In the case of *wl/wl* mice, H&E stained retinas were used to count the rows of photoreceptors in the outer nuclear layer and measure the outer segment length.

Phagocytosis Assay

The procedure for growing RPE cells on a Transwell filter was performed exactly as described (Gibbs et al., 2003). Briefly, RPE cells were isolated from 10- to 15-day-old WT mice. Eyes were digested using 2% Dispase (Sigma, Oakville, ON) and sheets of RPE cells were isolated and dispersed into growth medium containing DMEM, 10% bovine FCS, 1% penicillin/streptomycin, 2.5 mM L-glutamine, 1× MEM non-essential amino acids. All cell culture materials were obtained from Invitrogen. RPE cells were grown until confluent at 37℃, 5% CO_2. Equal amounts of WT and knockout outer segments were added to the RPE cells in growth medium and incubated at 37℃, 5% CO_2 for 60 minutes. RPE cells were washed three times with growth medium and incubated for an additional 60 minutes and then fixed in 4% paraformaldehyde. Bound outer segments were labeled with the rhodopsin Rho-4D2 antibody followed by an Alexa-Fluor-488-conjugated goat anti-mouse antibody. RPE cells were permeabilized with 47.5% ethanol. Internalized outer segments were labeled with the rhodopsin 4D2 antibody (Laird and Molday, 1988) and an Alexa-Fluor-594-conjugated goat anti-mouse antibody.

Rhodopsin and retinoid quantitative analysis

All procedures were conducted under dim red light as described (Liang et al., 2004). Typically two eyes were used for each experiment. The lens was removed and the eyes were cut into several small pieces and homogenized in a Dounce homogenizer ~20 times in 1 ml of 20 mM HEPES, pH 7.5, 150 mM NaCl, 5 mM hydroxylamine and 1% DDM and stirred for 1 hour at 4℃. Insoluble material was pelleted at 100,000 ***g*** for 10 minutes. The absorption spectra were acquired before and after a 10 minute bleach with light. The rhodopsin concentration was determined by the decrease in absorbance at 500 nm using a molar extinction coefficient of 40,000 M^{-1} cm^{-1}. In parallel, an aliquot was taken for analysis of opsin by western blotting. Retinoids were extracted from two eyes by homogenization six times in 2 ml of 50 mM MOPS, pH 6.5, 10 mM hydroxylamine and 50% ethanol and incubated for 30 minutes to allow formation of retinal oximes. Retinoids were extracted three times with 4 ml of hexane, dried with N_2, dissolved in 100 µl of hexane, and analyzed on an Agilent HPLC 1100 (Agilent Technologies, Mississauga, ON) using a silica column (Supelcosil LC-Si, 150 × 4.5 mm). Retinoids were separated by normal phase with 10% ethyl acetate, 90% hexane at a flow rate of 1.0 ml/min. Retinoids were identified by comparison with known standards.

Quantification of phospholipids

Lipids were extracted according to the method of Bligh and Dyer (Bligh and Dyer, 1959), separated by thin layer chromatography in $CHCl_3$:MeOH:NH_4OH (65:25:4) followed by a second dimension in $CHCl_3$:CH_3COOH:MeOH:H_2O (75:25:5:2.2) and quantified by measurement of the phosphorus content (Zhou and Arthur, 1992).

Auditory brainstem response (ABR)

Hearing in mice was assessed by ABR threshold analysis. Mice were anesthetized with an intraperitoneal injection of tribromoethanol (2.5 mg tribromoethanol/10 g body weight) and then placed on a heating pad in a sound-attenuating chamber. Recording electrodes (Model F-E2, Astro-Med, Inc.) were placed just under the skin, with the active electrode placed between the ears just above the vertex of the skull, the ground electrode between the eyes, and the reference electrode underneath the left ear. High-frequency transducers were placed just inside the ear canal and computer-generated sound stimuli were presented to both ears at defined intervals. Stimulus-evoked signals were recorded in an ABR recording system (Intelligent Hearing System, IHS, Miami, FL). Thresholds were determined for broadband click and 8 kHz, 16 kHz and 32 kHz pure-tone stimuli by increasing the sound pressure level (SPL) in 10 dB increments followed by 5 dB increases and decreases to determine the lowest level at which a distinct ABR wave pattern could be recognized.

Acknowledgements

The authors would like to thank Andrew Metcalfe and Jennifer Ryan for expert technical assistance with ERG recordings, Jesse Hammer for assembly of the

auditory figure and Dr Wayne Vogl for assistance with light microscopy. We would also like to acknowledge Scientific Services at The Jackson Laboratory.

Competing interests
The authors declare no competing interests.

Author contributions
J.A.C., X.Z., H.R.D., L.L.M., R.S.S., R.T.L. carried out the experiments. J.A.C., X.Z., R.S.M. and S.W.M.J. designed the experiments. J.A.C., R.S.M. and S.W.M.J. wrote the manuscript.

Funding
This work was supported by grants from the Canadian Institutes for Health Research [grant number MOP-106667 to R.S.M.]; the National Institutes of Health [grant number EY02422 to R.S.M.; EY11721 to S.W.M.J.]; Pew Charitable Trust [S.W.M.J.]; National Science Foundation of China [grant number 81271007 to X.Z.]. J.A.C. was supported by a National Sciences and Engineering Council predoctoral studentship. R.S.M. holds a Canada Research Chair in Vision and Macular Degeneration. S.W.M.J. is an Investigator of the Howard Hughes Medical Institute. Deposited in PMC for release after 6 months.

Supplementary material
Supplementary material available online at
http://jcs.biologists.org/lookup/suppl/doi:10.1242/jcs.145052/-/DC1

References
Bligh, E. G. and Dyer, W. J. (1959). A rapid method of total lipid extraction and purification. *Can. J. Biochem. Physiol.* **37**, 911-917.
Boesze-Battaglia, K., Organisciak, D. T. and Albert, A. D. (1994). RCS rat retinal rod outer segment membranes exhibit different cholesterol distributions than those of normal rats. *Exp. Eye Res.* **58**, 293-300.
Cacciagli, P., Haddad, M. R., Mignon-Ravix, C., El-Waly, B., Moncla, A., Missirian, C., Chabrol, B. and Villard, L. (2010). Disruption of the ATP8A2 gene in a patient with a t(10;13) de novo balanced translocation and a severe neurological phenotype. *Eur. J. Hum. Genet.* **18**, 1360-1363.
Cheng, C. L., Djajadi, H. and Molday, R. S. (2013). Cell-specific markers for the identification of retinal cells by immunofluorescence microscopy. *Methods Mol. Biol.* **935**, 185-199.
Coleman, J. A. and Molday, R. S. (2011). Critical role of the beta-subunit CDC50A in the stable expression, assembly, subcellular localization, and lipid transport activity of the P4-ATPase ATP8A2. *J. Biol. Chem.* **286**, 17205-17216.
Coleman, J. A., Kwok, M. C. and Molday, R. S. (2009). Localization, purification, and functional reconstitution of the P4-ATPase Atp8a2, a phosphatidylserine flippase in photoreceptor disc membranes. *J. Biol. Chem.* **284**, 32670-32679.
Coleman, J. A., Quazi, F. and Molday, R. S. (2013). Mammalian P(4)-ATPases and ABC transporters and their role in phospholipid transport. *Biochim Biophys Acta* **1831**, 555-574.
Cook, N. J., Molday, L. L., Reid, D., Kaupp, U. B. and Molday, R. S. (1989). The cGMP-gated channel of bovine rod photoreceptors is localized exclusively in the plasma membrane. *J. Biol. Chem.* **264**, 6996-6999.
Darland-Ransom, M., Wang, X., Sun, C. L., Mapes, J., Gengyo-Ando, K., Mitani, S. and Xue, D. (2008). Role of C. elegans TAT-1 protein in maintaining plasma membrane phosphatidylserine asymmetry. *Science* **320**, 528-531.
Emre, O. E., Gulsuner, S., Bilguvar, K., Nazli Basak, A., Topaloglu, H., Tan, M., Tan, U., Gunel, M. and Ozcelik, T. (2012). Missense mutation in the ATPase, aminophospholipid transporter protein ATP8A2 is associated with cerebellar atrophy and quadrupedal locomotion. *Eur. J. Hum. Genet.* **21,** 281-285.
Fliesler, S. J. and Anderson, R. E. (1983). Chemistry and metabolism of lipids in the vertebrate retina. *Prog. Lipid Res.* **22**, 79-131.
Gibbs, D., Kitamoto, J. and Williams, D. S. (2003). Abnormal phagocytosis by retinal pigmented epithelium that lacks myosin VIIa, the Usher syndrome 1B protein. *Proc. Natl. Acad. Sci. USA* **100**, 6481-6486.
Gibson, N. J. and Brown, M. F. (1991). Role of phosphatidylserine in the MI-MII equilibrium of rhodopsin. *Biochem. Biophys. Res. Commun.* **176**, 915-921.
Graham, T. R. and Kozlov, M. M. (2010). Interplay of proteins and lipids in generating membrane curvature. *Curr. Opin. Cell Biol.* **22**, 430-436.
Hawkins, R. K., Jansen, H. G. and Sanyal, S. (1985). Development and degeneration of retina in rds mutant mice: photoreceptor abnormalities in the heterozygotes. *Exp. Eye Res.* **41**, 701-720.
Hessel, E., Herrmann, A., Müller, P., Schnetkamp, P. P. and Hofmann, K. P. (2000). The transbilayer distribution of phospholipids in disc membranes is a dynamic equilibrium evidence for rapid flip and flop movement. *Eur. J. Biochem.* **267**, 1473-1483.
Hicks, D. and Molday, R. S. (1986). Differential immunogold-dextran labeling of bovine and frog rod and cone cells using monoclonal antibodies against bovine rhodopsin. *Exp. Eye Res.* **42**, 55-71.
Humphries, M. M., Rancourt, D., Farrar, G. J., Kenna, P., Hazel, M., Bush, R. A., Sieving, P. A., Sheils, D. M., McNally, N., Creighton, P. et al. (1997). Retinopathy induced in mice by targeted disruption of the rhodopsin gene. *Nat. Genet.* **15**, 216-219.
Krishna, A. G., Menon, S. T., Terry, T. J. and Sakmar, T. P. (2002). Evidence that helix 8 of rhodopsin acts as a membrane-dependent conformational switch. *Biochemistry* **41**, 8298-8309.
Kwok, M. C., Holopainen, J. M., Molday, L. L., Foster, L. J. and Molday, R. S. (2008). Proteomics of photoreceptor outer segments identifies a subset of SNARE and Rab proteins implicated in membrane vesicle trafficking and fusion. *Mol. Cell. Proteomics* **7**, 1053-1066.
Laird, D. W. and Molday, R. S. (1988). Evidence against the role of rhodopsin in rod outer segment binding to RPE cells. *Invest. Ophthalmol. Vis. Sci.* **29**, 419-428.
LaVail, M. M. (1976). Rod outer segment disk shedding in rat retina: relationship to cyclic lighting. *Science* **194**, 1071-1074.
Levano, K., Punia, V., Raghunath, M., Debata, P. R., Curcio, G. M., Mogha, A., Purkayastha, S., McCloskey, D., Fata, J. and Banerjee, P. (2012). Atp8a1 deficiency is associated with phosphatidylserine externalization in hippocampus and delayed hippocampus-dependent learning. *J. Neurochem.* **120**, 302-313.
Liang, Y., Fotiadis, D., Maeda, T., Maeda, A., Modzelewska, A., Filipek, S., Saperstein, D. A., Engel, A. and Palczewski, K. (2004). Rhodopsin signaling and organization in heterozygote rhodopsin knockout mice. *J. Biol. Chem.* **279**, 48189-48196.
Mason, W. T., Fager, R. S. and Abrahamson, E. W. (1973). Lipid and fatty acid composition of frog photoreceptor outer segments. *Biochemistry* **12**, 2147-2150.
Menon, I., Huber, T., Sanyal, S., Banerjee, S., Barré, P., Canis, S., Warren, J. D., Hwa, J., Sakmar, T. P. and Menon, A. K. (2011). Opsin is a phospholipid flippase. *Curr. Biol.* **21**, 149-153.
Miljanich, G. P., Nemes, P. P., White, D. L. and Dratz, E. A. (1981). The asymmetric transmembrane distribution of phosphatidylethanolamine, phosphatidylserine, and fatty acids of the bovine retinal rod outer segment disk membrane. *J. Membr. Biol.* **60**, 249-255.
Molday, R. S. and Molday, L. L. (1987). Differences in the protein composition of bovine retinal rod outer segment disk and plasma membranes isolated by a ricin-gold-dextran density perturbation method. *J. Cell Biol.* **105**, 2589-2601.
Molday, R. S., Hicks, D. and Molday, L. (1987). Peripherin. A rim-specific membrane protein of rod outer segment discs. *Invest. Ophthalmol. Vis. Sci.* **28**, 50-61.
Natochin, M., Gasimov, K. G., Moussaif, M. and Artemyev, N. O. (2003). Rhodopsin determinants for transducin activation: a gain-of-function approach. *J. Biol. Chem.* **278**, 37574-37581.
Papermaster, D. S. and Dreyer, W. J. (1974). Rhodopsin content in the outer segment membranes of bovine and frog retinal rods. *Biochemistry* **13**, 2438-2444.
Poincelot, R. P. and Abrahamson, E. W. (1970). Phospholipid composition and extractability of bovine rod outer segments and rhodopsin micelles. *Biochemistry* **9**, 1820-1825.
Pomorski, T., Lombardi, R., Riezman, H., Devaux, P. F., van Meer, G. and Holthuis, J. C. (2003). Drs2p-related P-type ATPases Dnf1p and Dnf2p are required for phospholipid translocation across the yeast plasma membrane and serve a role in endocytosis. *Mol. Biol. Cell* **14**, 1240-1254.
Puts, C. F. and Holthuis, J. C. (2009). Mechanism and significance of P4 ATPase-catalyzed lipid transport: lessons from a Na+/K+-pump. *Biochim. Biophys. Acta* **1791**, 603-611.
Ruggiero, L., Connor, M. P., Chen, J., Langen, R. and Finnemann, S. C. (2012). Diurnal, localized exposure of phosphatidylserine by rod outer segment tips in wild-type but not Itgb5-/- or Mfge8-/- mouse retina. *Proc. Natl. Acad. Sci. USA* **109**, 8145-8148.
Sebastian, T. T., Baldridge, R. D., Xu, P. and Graham, T. R. (2012). Phospholipid flippases: building asymmetric membranes and transport vesicles. *Biochim. Biophys. Acta* **1821**, 1068-1077.
Stapelbroek, J. M., Peters, T. A., van Beurden, D. H., Curfs, J. H., Joosten, A., Beynon, A. J., van Leeuwen, B. M., van der Velden, L. M., Bull, L., Oude Elferink, R. P. et al. (2009). ATP8B1 is essential for maintaining normal hearing. *Proc. Natl. Acad. Sci. USA* **106**, 9709-9714.
Sung, C. H. and Chuang, J. Z. (2010). The cell biology of vision. *J. Cell Biol.* **190**, 953-963.
Tsang, S. H., Burns, M. E., Calvert, P. D., Gouras, P., Baylor, D. A., Goff, S. P. and Arshavsky, V. Y. (1998). Role for the target enzyme in deactivation of photoreceptor G protein in vivo. *Science* **282**, 117-121.
van der Mark, V. A., Elferink, R. P. and Paulusma, C. C. (2013). P4 ATPases: Flippases in Health and Disease. *Int. J. Mol. Sci.* **14**, 7897-7922.
van der Velden, L. M., Wichers, C. G., van Breevoort, A. E., Coleman, J. A., Molday, R. S., Berger, R., Klomp, L. W. and van de Graaf, S. F. (2010). Heteromeric interactions required for abundance and subcellular localization of human CDC50 proteins and class 1 P4-ATPases. *J. Biol. Chem.* **285**, 40088-40096.
Wu, G. and Hubbell, W. L. (1993). Phospholipid asymmetry and transmembrane diffusion in photoreceptor disc membranes. *Biochemistry* **32**, 879-888.
Wu, Y., Tibrewal, N. and Birge, R. B. (2006). Phosphatidylserine recognition by phagocytes: a view to a kill. *Trends Cell Biol.* **16**, 189-197.
Xu, Q., Yang, G. Y., Liu, N., Xu, P., Chen, Y. L., Zhou, Z., Luo, Z. G. and Ding, X. (2012). P4-ATPase ATP8A2 acts in synergy with CDC50A to enhance neurite outgrowth. *FEBS Lett.* **586**, 1803-1812.
Zhou, X. and Arthur, G. (1992). Improved procedures for the determination of lipid phosphorus by malachite green. *J. Lipid Res.* **33**, 1233-1236.
Zhu, X., Libby, R. T., de Vries, W. N., Smith, R. S., Wright, D. L., Bronson, R. T., Seburn, K. L. and John, S. W. (2012). Mutations in a P-type ATPase gene cause axonal degeneration. *PLoS Genet.* **8**, e1002853.